PAPERS | FEBRUARY 01 2017

Weight of an hourglass—Theory and experiment in quantitative comparison VIDEO

Achim Sack; Thorsten Pöschel

Am. J. Phys. 85, 98–107 (2017)
https://doi.org/10.1119/1.4973527

Weight of an hourglass—Theory and experiment in quantitative comparison

Achim Sack and Thorsten Pöschel
Institute for Multiscale Simulation, Universität Erlangen-Nürnberg, Nägelsbachstraße 49b, 91052 Erlangen, Germany

(Received 3 March 2016; accepted 16 December 2016)

A flowing hourglass changes its weight in the course of time because of the accelerated motion of its center of mass. While this insight is not new, it is frequently said that the effect is tiny and hardly measurable. Here, we present a simple experiment that allows the monitoring of weight as a function of time, and that shows that there are different stages of the weight variation. The experimental result is in quantitative agreement with theory. [http://dx.doi.org/10.1119/1.4973527]

I. INTRODUCTION

The question whether or not the weight, shown by a scale, of a running hourglass differs from the weight of the hourglass at rest is of great pedagogical value since experience shows that this question leads to controversial and instructive discussions. In our opinion, it teaches that a systematic analysis of a physical situation is superior to a phenomenological analysis, in a certain sense.

Phenomenologically, when the sand starts pouring part of it is freely falling and is thus not supported by the scale, which leads to a reduced weight shown by the scale. But when the grains arrive at the bottom, they come to rest in the lower chamber by transferring momentum and, consequently, force to the balance. A simple calculation[1] shows that these two effects cancel out; thus, it may be argued that except for short intervals of time at the very beginning and at the very end of the flow, the scale shows the same weight as if the sand were at rest. It has been shown that this argument is wrong (or insufficient);[2–5] nevertheless, it is still taught in high schools and universities. Interestingly, this flawed solution can be found in well recognized textbooks and journals (e.g., Refs. 6–10, to mention just a few out of many), and it even made it to the National Physics Olympiad of Singapore.[11]

A related problem is the change of weight of an Atwood machine when it is in motion. This classical experiment by Poggendorff[12] (repeated many times in the literature, e.g., Refs. 13 and 14) can be explained easily by evaluating the acceleration of the center of mass. Thus, the idea that leads us immediately to the correct solution is simple: look to the acceleration of the center of mass of the hourglass! This more systematic approach reveals that the solution sketched above fails at least for the following arguments:

(i) The material in the upper and lower containers, as well as in the freely falling stream of sand, is not at rest, and sand of time-dependent mass moves with a certain velocity determined by the outflow rate and the geometry of the container. Thus, in the course of time, moving material (in the upper container) comes to rest at a different location (in the lower container), which implies an acceleration.

(ii) At a given time t, during the small interval of time dt, sand moves effectively from a certain height h_u in the upper container to a height h_l in the lower container (see Fig. 1), where $h_u - h_l$ is a decreasing function of time. This corresponds to an acceleration whose time dependence is determined by the geometrical shape of the hourglass.

From the analysis of the motion of the center of mass,[2–5] it follows that the weight of the hourglass is a function of time that depends on the specific details including the geometric shape of the hourglass, the outflow rate, and the angle of repose of the sand. In the literature, the effect was described as tiny, perhaps smaller than the change of gravity when turning the hourglass over and thereby changing the distance of the center of mass of the sand from the center of Earth,[3] an effect that is on the order of some μg and cannot be measured with usual physics lab equipment. Even in an experiment with a very large device of height 120 cm, emptying in only 10 s, a maximal change in weight of only 49 mg was measured,[2] and the time dependence of this effect could not be determined. Using a multiple-orifice setup[5] where the upper cylindrical container was separated from the lower cylindrical container by a sieve, a quantitative measurement was presented. For the given geometry, however, a constant increase of the weight is expected from theory whereas the measurement shows a clear trend that may be understood either from the large uncertainty (error bars) of the measurement or from the non-stationary flow rate. Indeed, unlike fluids granular matter shows flows at a rate independent of the filling height. Whether this result, shown for a single orifice using different approaches,[15–17] holds true also for flow

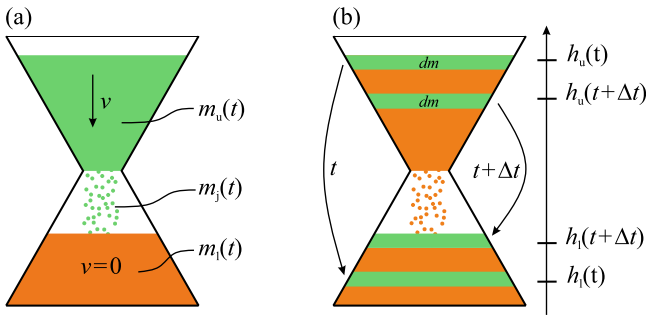

Fig. 1. (color online) (a) In an hourglass, the mass of moving material in the upper container and in the stream sand changes over the course of time. This material comes to rest in the lower container, exerting a force during deceleration. (b) In the regime of steady flow, during time dt the mass dm is effectively transferred from $h_u(t)$ to $h_l(t)$, where $\Delta h \equiv h_u - h_l$ is a function of time and depends on the geometry of the hourglass. This transfer involves accelerated motion of mass and, thus, a time-dependent force.

through a sieve remains unclear. But even for the simplified experiment[5] the full time dependence of the change of weight could not be measured due to perturbations of the opening mechanism.

In this paper, we present experimental results that show that the difference of weight of a flowing hourglass, in comparison with the same hourglass in which the sand is at rest, is clearly measurable, even with simple equipment. When measuring the weight of the hourglass as a function of time, we observe different stages of behavior that can be understood qualitatively in comparison with a high speed video recording. While the simple phenomenological argument mentioned above fails to explain the change of weight, by means of a systematic analysis of the physical process (namely, the accelerated motion of the center of mass) we derive a theoretical description without any free parameters that is in *quantitative* agreement with the experiment.

In Secs. II and III, we will present the experimental results and the corresponding theory, respectively. Section IV discusses the stages of the flow apparent in the time dependence of the change of weight of the hourglass. Unlike earlier references, this paper will show that even with simple equipment the weight of the hourglass can be measured as a function of time, and that this time dependence can be explained theoretically.

II. EXPERIMENT

The experiment is shown in Fig. 2. The upper container consists of a cylinder and a cone characterized by $R_1 = 2.75\,\text{cm}$, $R_2 = 1.0\,\text{cm}$, and $z_2 = 3.5\,\text{cm}$, initially filled up to $z_1 = 8.2\,\text{cm}$ with $M = 800\,\text{g}$ bronze powder (our "sand") of density $\rho = 5,230\,\text{kg/m}^3$, a grain size of approximately $150\,\mu\text{m}$, and angle of repose $\alpha = 28.3°$. This filling material was chosen for its high density and in order to avoid electrical charging of the material that might disrupt homogeneous flow. The lower compartment consists of a cylinder characterized by $R_3 = 2.75\,\text{cm}$ and $z_3 = -21.5\,\text{cm}$. Both upper and lower compartments are manufactured from polycarbonate material. Unlike common hourglasses, the upper and lower vessels were not sealed, in order to avoid a difference of air pressure in the upper and lower compartments; in closed, non-evacuated hourglasses the flow of sand through the orifice carries a small amount of air with it leading to increased pressure in the lower chamber.[18] It has been shown that the counter-flowing air leads to unsteady flow, termed "ticking of hourglasses," which has been extensively studied in the literature.[19–22] The open construction of our experiment avoids pressure differences caused by flowing air and thus provides a steady flow of sand at rate $F = 720\,\text{g/s}$.

The hourglass was placed on a scale using a load cell with 2 kg capacity (LCB70, ME-Meßsysteme). The electrical signal from the strain gauge of the load cell was amplified and digitized using an ADS1281 analog-to-digital converter. The weight of the hourglass was sampled at a rate of 250 Hz.

Initially, the orifice of the upper container was closed by a lid held by an electromagnet. At time $t = 0$, the orifice was opened and the pouring of the sand led to an accelerated motion of the center of mass, and thus to a change in the weight measured by the scale. Figure 3 shows the weight of the hourglass during the run, with the weight of the apparatus subtracted (this figure is enhanced online with a movie of the experiment). A running average over six consecutive force measurements was applied. It is worth mentioning that the

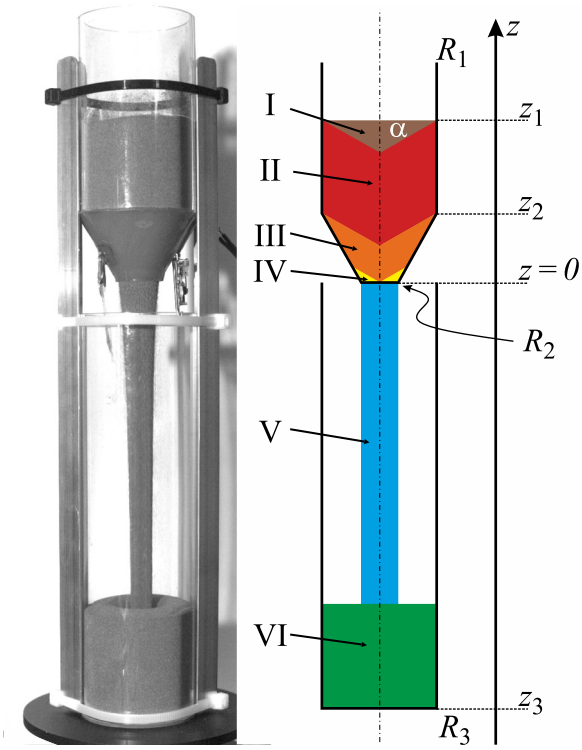

Fig. 2. (color online) Experimental setup (left). The sketch (right) introduces the geometric parameters, defines the sub-volumes I–VI, and shows α, the angle of repose. The sketch shows a cut through the symmetry axis.

experiment is highly reproducible; the deviations between independent repetitions of the experiment are tiny. These deviations and all the fine structure of the data are no more than the line width of the curve in Fig. 3.

The details of the experimental result will be discussed below. In Sec. III, we compute the weight of the hourglass theoretically with some model assumptions. Note that the theory presented does not contain any free parameters. Comparing experiment and theory in Sec. IV, we obtain quantitative agreement. Noticeable deviations between the experiment and theory can be seen only in the very beginning and very end of the experiment. These deviations are due to model assumptions, are well understood, and will be discussed in detail in Sec. IV.

III. MODEL

A. Geometry

The geometry of our model hourglass is sketched in Fig. 2. As for a typical hourglass, the upper container consists of a cone and a cylinder and the lower container has the same shape as the upper container. For the model presented here, we assume that the total volume of the sand only fills the cylindrical portion of the lower container, so that we do not need to include the cone of the lower part in our calculation.

Our strategy for the computation of the vertical position of the center of mass (COM), $Z(t)$, is to subdivide the volume into geometrical primitives such as cylinders, cones, and annuli, whose geometrical extensions are known for each time t of operation. The mass and center of mass of these primitives are either known or can be obtained by combining other primitives of positive and negative mass. The coordinate of the

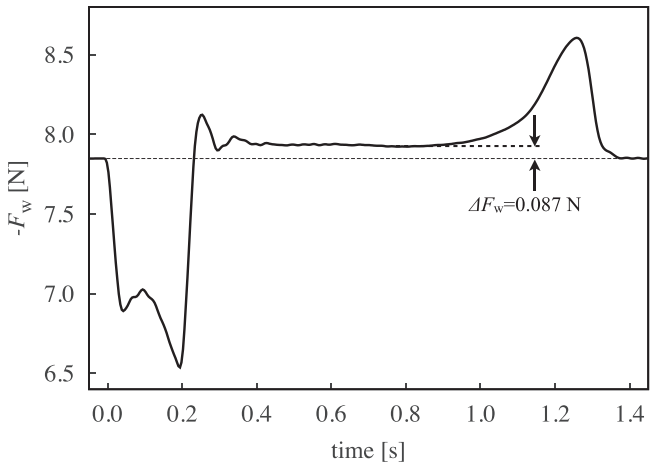

Fig. 3. Weight of the granulate inside the hourglass as a function of time (the weight of the apparatus has been subtracted). At time $t=0$, the orifice opens. We observe a characteristic evolution that can be understood in detail from the theory presented in Sec. III. The dashed line shows the increase in weight due to the accelerated motion of the center of mass (enhanced online) [URL: http://dx.doi.org/10.1119/1.4973527.1].

center of mass of the hourglass as a function of time is then obtained from the combination of the masses and centers of mass of the primitives.

Following this strategy, as illustrated in Fig. 2, we subdivide the volume into sub-volumes I–VI of time-dependent mass $m_i(t)$ and center of mass $Z_i(t)$, with $i = \mathrm{I}, \ldots, \mathrm{VI}$, so that the overall COM of the sand is

$$Z(t) = \frac{\sum_{i=\mathrm{I}}^{\mathrm{VI}} Z_i(t) m_i(t)}{\sum_{i=\mathrm{I}}^{VI} m_i(t)} = \frac{1}{M} \sum_{i=\mathrm{I}}^{\mathrm{VI}} Z_i(t) m_i(t), \tag{1}$$

where M is the total mass of the sand. Knowing $Z(t)$ as an analytic function, we can compute the time-dependent force acting on the balance as

$$F_w = M\left(g + \frac{\mathrm{d}^2 Z(t)}{\mathrm{d}t^2}\right). \tag{2}$$

The masses and centers of mass of the sub-volumes are functions of time of the form

$$m_i(t) = \begin{cases} m_i^0 = \text{const.} & \text{for } t \le t_i^0 \\ m_i'(t) & \text{for } t_i^0 \le t \le t_i^e \\ m_i^e = \text{const.} & \text{for } t \ge t_i^e, \end{cases} \tag{3}$$

$$Z_i(t) = \begin{cases} Z_i^0 = \text{const.} & \text{for } t \le t_i^0 \\ Z_i'(t) & \text{for } t_i^0 \le t \le t_i^e \\ Z_i^e = \text{const.} & \text{for } t \ge t_i^e, \end{cases} \tag{4}$$

where $i = \mathrm{I} \ldots \mathrm{VI}$ and t_i^0 and t_i^e are, respectively, the times for each sub-volume at which the flow starts and stops. For the initial conditions, we assume that the upper container is filled up to the height z_1 and the upper surface of the granular material is flat. At time $t=0$, the material starts flowing through the orifice at rate F. In contrast to a fluid, the granular-material flow rate F is independent of filling height.[23–33] (The independence of pressure on filling height is known as Janssen's law;[34] the independence of flow rate as Beverloo's law.[15]) The functional form of the flow rate (Beverloo's law) follows from a dimensional analysis, and is given by[35,36]

$$F = \frac{dm}{dt} = C_F \sqrt{g} \rho A^{5/2}, \tag{5}$$

with C_F a dimensionless constant, g the gravitational field strength, ρ the material density, and A the cross-sectional area of the orifice. In this paper, we assume that the flow rate F is independent of time as long as sand flows. This is a good approximation except, perhaps, for the very first instant where the acceleration of the granulate is limited by its inertia, and the very last moment when the filling height of the upper container is on the order of the diameter of the orifice. For the quantitative comparison in Sec. IV, we measured the value of F under this assumption.

In Secs. III B–III F, we compute m_i and Z_i and the corresponding times t_i^0 and t_i^e for all sub-volumes, and subsequently, in Sec. IV, the function $Z(t)$ and the corresponding weight of the hourglass. For these calculations, we will introduce the time-dependent filling level $z(t)$, defined as the highest vertical position occupied by sand, and some temporary variables, indicated by an asterisk (e.g., x^*). Such variables are only relevant in the context of the present section.

For the quantitative plots, we take the parameter values: $g = 9.81\,\mathrm{m/s^2}, \rho = 5{,}230\,\mathrm{kg/m^3}$, $R_1 = 2.75\,\mathrm{cm}, R_2 = 1.0\,\mathrm{cm}$, $z_1 = 8.2\,\mathrm{cm}, z_2 = 3.5\,\mathrm{cm}$, $\alpha = 28.3^\circ$, and $F = 0.69\,\mathrm{kg/s}$, in agreement with the experiment described in Sec. II.

B. Sub-volume I

At the initial time, $t=0$, sub-volume I (see Fig. 2) has the shape of a cone. This gives us

$$\begin{aligned} &m_I^0 = \frac{\rho\pi}{3} R_1^3 \tan\alpha; \quad t_I^0 = 0; \quad t_I^e = \frac{m_I^0}{F}, \\ &m_I^e = 0; \quad m_I'(t) = m_I^0 - Ft; \quad Z_I^0 = z_1 - \frac{1}{4} R_1 \tan\alpha. \end{aligned} \tag{6}$$

There are two possible scenarios for the emptying of sub-volume I: In case (a), shown in Fig. 4(a), a crater of constant slope α forms in the middle of the sub-volume. The crater grows until its radius approaches R_1 at $t = t_1^e$. In case (b), shown in Fig. 4(b), a crater of radius R_1 and increasing depth forms. At $t = t_1^e$, its slope approaches the angle of repose α. For both cases, we describe the body of mass $m_1'(t)$ sketched in Fig. 4 as a superposition of the initial cone whose mass and center of mass given in Eq. (6) and the cone of (negative) mass $m^*(t) = -Ft$ and COM

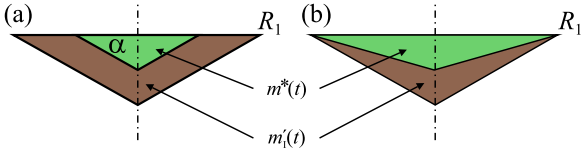

Fig. 4. Scenarios (a) and (b) for the outflow of sub-volume I.

$$Z^*(t) = \begin{cases} z_1 - \frac{1}{4}\left(\frac{3F\tan^2\alpha}{\rho\pi}\right)^{1/3} t^{1/3} & \text{case(a)} \\ z_1 - \frac{3}{4}\frac{F}{\rho\pi R_1^2} t & \text{case(b)}. \end{cases} \tag{7}$$

The COM of sub-volume I for $t_{\mathrm{I}}^0 \le t \le t_{\mathrm{I}}^{\mathrm{e}}$ is then

$$Z_{\mathrm{I}}'(t) = \frac{1}{m_{\mathrm{I}}'(t)}\left[Z_{\mathrm{I}}^0 m_{\mathrm{I}}^0 + Z^*(t)m^*(t)\right]. \tag{8}$$

Figure 5 shows Z_{I} for both cases. It may be surprising that the limits $t \to t_{\mathrm{I}}^{\mathrm{e}}$ are different for the two cases. When we express for case (a) $Z_{\mathrm{I}}'(t)$ as a function of the instantaneous radius r^* of the smaller cone we obtain

$$Z_{\mathrm{I}}^{\mathrm{e}} = \lim_{r^*\to R_1}\left[z_1 - \frac{\tan\alpha}{4}\frac{R_1^4 - (r^*)^4}{R_1^3 - (r^*)^3}\right] = z_1 - \frac{R_1\tan\alpha}{3}. \tag{9}$$

For case (b), we express $Z_{\mathrm{I}}(t)$ in terms of the position z of the tip of the smaller cone, and here we obtain

$$\begin{aligned} Z_{\mathrm{I}}^{\mathrm{e}} &= \lim_{z\to z_1 - R_1\tan\alpha}\left[z_1 - \frac{1}{4}(z_1 - R_1\tan\alpha - z)\right] \\ &= z_1 - \frac{R_1\tan\alpha}{2}. \end{aligned} \tag{10}$$

The different limits (see Fig. 5) are an interesting mathematical peculiarity that has its origin ultimately in the continuum description of granular matter, which is problematic in the limit of mass approaching zero. This issue is not a problem for our calculation, however, because the mass vanishes $m_{\mathrm{I}}(t) \to 0$ as $t \to t_{\mathrm{I}}^{\mathrm{e}}$, and therefore the product $m_{\mathrm{I}}(t)Z_{\mathrm{I}}(t)$ does not contribute to Eq. (1) for $t \to t_{\mathrm{I}}^{\mathrm{e}}$.

C. Sub-volume II

Initially, sub-volume II (see Fig. 2) consists of a cylinder of height $z_1 - z_2$ and radius R_1, closed at the top by a cone of negative mass and an identical cone, but of positive mass, at the floor. For this sub-volume we have

$$\begin{aligned} &m_{\mathrm{II}}^0 = \rho\pi R_1^2(z_1 - z_2); \quad t_{\mathrm{II}}^0 = t_I^{\mathrm{e}}; \quad t_{\mathrm{II}}^{\mathrm{e}} = t_{\mathrm{II}}^0 + \frac{m_{\mathrm{II}}^0}{F} \\ &m_{\mathrm{II}}'(t) = M_{\mathrm{II}}^0 - (t - t_{\mathrm{II}}^0)F; \quad m_{\mathrm{II}}^{\mathrm{e}} = 0. \end{aligned} \tag{11}$$

For $t_{\mathrm{II}}^0 \le t \le t_{\mathrm{II}}^{\mathrm{e}}$, the filling level reads

$$z(t) = z_1 - \frac{F}{\rho\pi R_1^2}(t - t_{\mathrm{II}}^0), \tag{12}$$

and we write for the COM of the cylinder

$$Z_{\mathrm{cyl}}^*(t) = \frac{z(t) + z_2}{2}. \tag{13}$$

For the upper (cu) and lower (cl) cones, we obtain

$$\begin{aligned} &m_{\mathrm{cu}}^* = -\frac{\rho\pi}{3}R_1^3\tan\alpha; \quad Z_{\mathrm{cu}}^*(t) = z(t) - \frac{R_1\tan\alpha}{4} \\ &m_{\mathrm{cl}}^* = -m_{\mathrm{cu}}^*; \quad Z_{\mathrm{cl}}^*(t) = z_2 - \frac{R_1\tan\alpha}{4}. \end{aligned} \tag{14}$$

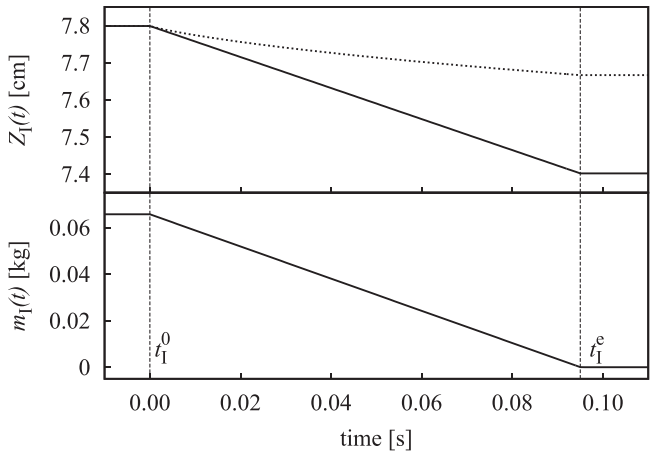

Fig. 5. Top: COM as functions of time for scenarios (a) (dotted line) and (b) (solid line); bottom: mass of sub-volume I as a function of time.

Consequently, we have that the COM is at

$$\begin{aligned} Z_{\mathrm{II}}' &= \frac{1}{m_{\mathrm{II}}'}\left[m_{\mathrm{II}}'Z_{\mathrm{cyl}}^* + m_{\mathrm{cu}}^*Z_{\mathrm{cu}}^* + m_{\mathrm{cl}}^*Z_{\mathrm{cl}}^*\right] \\ &= \frac{z(t) + z_2}{2} - \frac{R_1\tan\alpha}{3}, \end{aligned} \tag{15}$$

and in particular

$$Z_{\mathrm{II}}^0 = \frac{z_1 + z_2}{2} - \frac{R_1\tan\alpha}{3}; \quad Z_{\mathrm{II}}^{\mathrm{e}} = z_2 - \frac{R_1\tan\alpha}{3}. \tag{16}$$

Figure 6 shows the functions $Z_{\mathrm{II}}(t)$ and $m_{\mathrm{II}}(t)$.

D. Sub-volume III

Sub-volume III is located below sub-volume II; see Fig. 2 and the expanded details in Fig. 7, where the nomenclature used in this section is introduced. In Fig. 7, we define the conical segments $S_1, \ldots, S_4$, of negative and positive masses, whose superposition equals sub-volume III. Note that only S_3 and S_4 depend on time.

1. Segment S_1

Sub-volume S_1 (see Fig. 7) is a time-independent cone of positive mass with height and radius

$$z_a^* = \frac{R_2}{T}; \quad R(z_a^*) = \frac{z_a^*}{\tan\alpha}, \tag{17}$$

respectively, where we define for later reference

$$T \equiv \frac{1}{\tan\alpha} - \frac{R_1 - R_2}{z_2}. \tag{18}$$

Consequently, the mass and COM are

$$m_1^* = \frac{\rho\pi}{3\tan^2\alpha}\left(\frac{R_2}{T}\right)^3; \quad Z_1^* = \frac{3}{4}\frac{R_2}{T}. \tag{19}$$

2. Segment S_2

Segment S_2 is a time-independent cone of negative mass with the same radius as S_1 and height $z_a^* + z_2R_2/(R1 - R2)$, so that with Eq. (17) we have

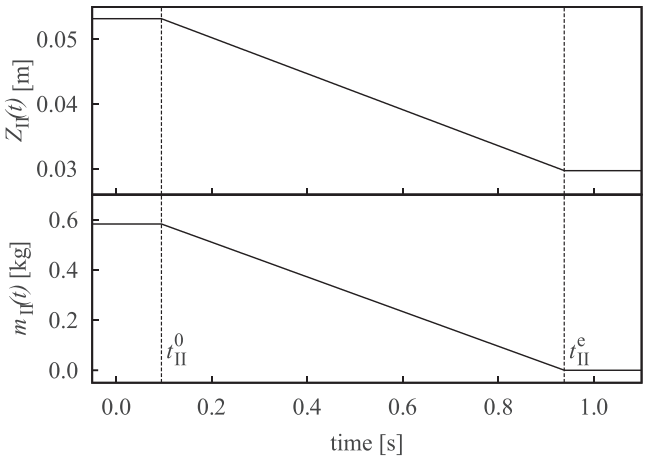

Fig. 6. COM (top) and mass (bottom) of sub-volume II as functions of time.

$$m_2^* = -\frac{\rho\pi}{3\tan^2\alpha}\left(\frac{R_2}{T}+\frac{z_2R_2}{R1-R2}\right)^3$$
$$Z_2^* = \frac{R_2}{T}-\frac{1}{4}\left(\frac{R_2}{T}+\frac{z_2R_2}{R1-R2}\right). \tag{20}$$

3. Segment S_3

Segment S_3, of negative mass, is a cone with radius $R(z)$ and height $R(z)\tan\alpha$; therefore, for $t^0_{III} = t^e_{II} \le t \le t^e_{III}$

$$m_3^*(z) = -\frac{\pi\rho}{3}\left[R_2+\frac{R1-R2}{z_2}z(t)\right]^3\tan\alpha$$
$$Z_3^*(z) = z(t)-\frac{\tan\alpha}{4}\left[R_2+\frac{R1-R2}{z_2}z(t)\right]. \tag{21}$$

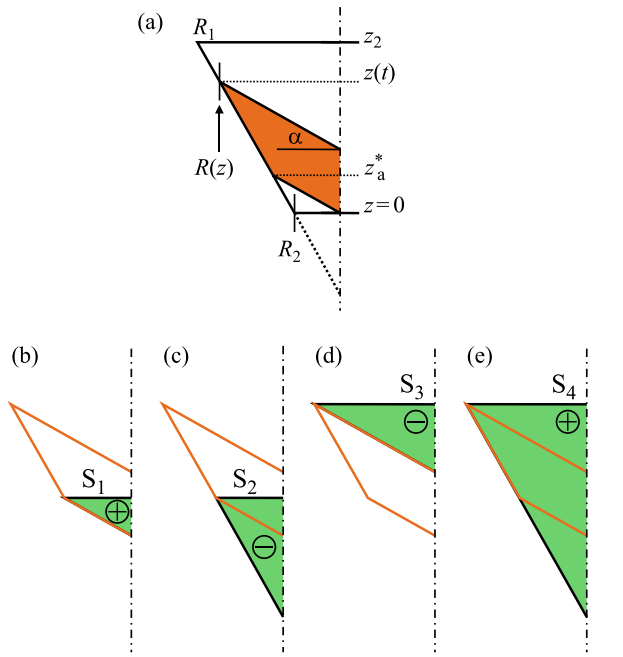

Fig. 7. (a) Sketch of sub-volume III to introduce the nomenclature. (b)–(e) Segments of volumes of positive ⊕ and negative ⊖ masses used in the calculation. Their superposition results in volume III.

The filling height $z(t)$ and t^e_{III} are computed later from the total mass of sub-volume III. For $t \to t^0_{III}$ when $z \to z_2$, we obtain

$$m_3^*(z_2) = -\frac{\pi\rho}{3}R_1^3\tan\alpha; \quad Z_3^*(z_2) = z_2-\frac{1}{4}\tan\alpha R_1. \tag{22}$$

4. Segment S_4

Segment S_4 is a cone of mass and COM given by

$$m_4^*(z) = \frac{\pi\rho}{3}\left[R_2+\frac{R_1-R_2}{z_2}z(t)\right]^2\left[z(t)+\frac{z_2R_2}{R_1-R_2}\right],$$
$$Z_4^*(z) = \frac{3}{4}z(t)-\frac{1}{4}\frac{z_2R_2}{R_1-R_2}. \tag{23}$$

The first bracketed expression in Eq. (23) specifies the radius $R(z(t))$ of the cone, and the second bracketed expression, its height. The initial mass and COM, for $z \to z_2$, are

$$m_4^*(z_2) = \frac{\pi\rho}{3}R_1^2z_2\left[1+\frac{R_2}{R_1-R_2}\right]$$
$$Z_4^*(z_2) = \frac{z_2}{4}\left[3-\frac{R_2}{R_1-R_2}\right]. \tag{24}$$

5. Mass and COM of sub-volume III

Using the results of Secs. III D 1–III D 4, we compute the mass and COM of sub-volume III by superposition of the segments $S_1, \ldots, S_4$. From the initial mass in sub-volume III, we have that

$$m^0_{III} = m_1^* + m_2^* + m_3^*(z_2) + m_4^*(z_2) = F\,(t^e_{III} - t^0_{III}), \tag{25}$$

and because m^e_{III} obviously vanishes, we obtain the time t^e_{III}. The total mass as a function of time then follows from:

$$m_{III}(t) = m^0_{III} - F\,(t - t^0_{III}). \tag{26}$$

For the computation of the COM via the COMS of the segments,

$$Z'_{III}(t) = \frac{1}{m'_{III}(t)}\left[Z_1^*m_1^* + Z_2^*m_2^* + Z_3^*(z)m_3^*(z) + Z_4^*(z)m_4^*(z)\right], \tag{27}$$

we need the filling height $z(t)$, since m_3^*, m_4^*, Z_3^*, and Z_4^* depend on time through $z(t)$. The filling height can be found from

$$m_{III}(t) = m_1^* + m_2^* + m_3^*(z(t)) + m_4^*(z(t)), \tag{28}$$

with the segment masses given in Eqs. (19)–(21) and (23), and with the time-dependent mass given in Eq. (26). The left-hand side is a third-order polynomial of the filling height. By solving the third-order equation, we obtain $z(t)$ and subsequently Z'_{III} as an explicit function of time via Eq. (27). Figure 8 shows the resulting functions $Z_{III}(t)$ and $m_{III}(t)$.

E. Sub-volume IV

1. Time-independent flow rate

Sub-volume IV is a tiny annulus below sub-volume III, and which is hardly visible in Fig. 2. The magnification shown in Fig. 9 defines the variable z_a^*, which is the same as in Sec. III D. One can argue whether it is necessary to compute the contribution of this sub-volume since its mass is small and the computation requires some effort. We believe it is necessary for the sake of consistency. Recall that we need the second derivative of the COM to obtain the weight of the hourglass [see Eq. (2)]; thus, small rapidly changing masses may lead to significant contributions to the weight. For $t \ll t_{\mathrm{IV}}^0$, the area at $z=0$ is covered with sand such that Beverloo's law, Eq. (5), is a good approximation. For $t \approx t_{\mathrm{IV}}^0$, it is certainly not justified to assume constant flux F; however, in the absence of solutions in the literature for this situation, we here also assume constant flux F. Moreover, sub-volume IV is certainly tiny as compared to all other sub-volumes so that the details of the flow for this volume are of minor importance for the total weight of the hourglass, provided that the large jumps in the second derivatives, discussed above, are avoided.

2. Mass of sub-volume IV

Sub-volume IV combines a frustum (height $z(t)$, radii $R(z)$ and R_2) of positive mass and a frustum (height $z(t)$, radii $R(z)$ and R^*) of negative mass, as shown in Fig. 9. Its mass is, therefore,

$$\frac{m'_{\mathrm{IV}}(t)}{\rho\pi} = \frac{z}{3}\left[R^2(z) + R(z)R_2 + R_2^2\right] - \frac{z}{3}\left[R^2(z) + R(z)R^* + (R^*)^2\right] \tag{29}$$

with

$$R(z) = R_2 + z(R1 - R2)/z_2, \qquad R^* = R_2 - zT, \tag{30}$$

and with T defined in Eq. (18). The result for the mass is then

$$\frac{m_{\mathrm{IV}}(t)}{\rho\pi} = TR_2z^2 + \frac{1}{3}T\left(\frac{R_1 - R_2}{z_2} - T\right)z^3. \tag{31}$$

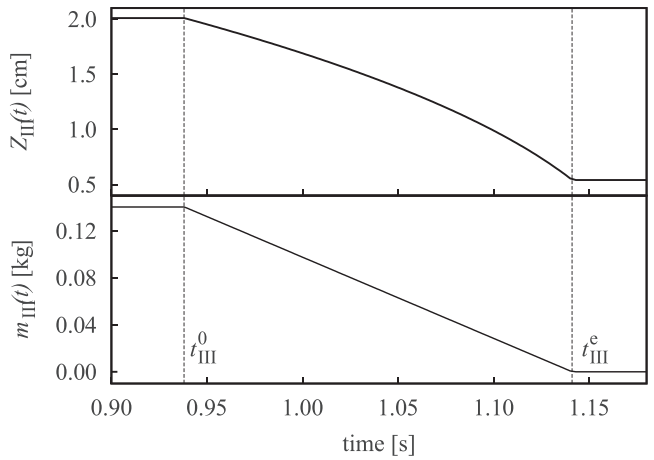

Fig. 8. COM and mass of sub-volume III as functions of time.

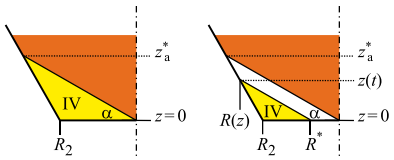

Fig. 9. Sketch of sub-volume IV at time $t \le t_{\mathrm{IV}}^0$ (left), and at a later time $t_{\mathrm{IV}}^0 < t < t_{\mathrm{IV}}^{\mathrm{e}}$ (right).

At time $t_{\mathrm{IV}}^0 = t_{\mathrm{III}}^{\mathrm{e}}$, we have $z = z_a^*$ and Eq. (31) simplifies to

$$m_{\mathrm{IV}}^0 = \rho\pi R_2^3\left(\frac{1}{T} - \frac{1}{3\tan\alpha T^2}\right). \tag{32}$$

We then find the mass of sub-volume IV to be

$$m'_{\mathrm{IV}}(t) = m_{\mathrm{IV}}^0 - F\left(t - t_{\mathrm{IV}}^0\right); \quad t_{\mathrm{IV}}^{\mathrm{e}} = t_{\mathrm{IV}}^0 + \frac{m_{\mathrm{IV}}^0}{F} \tag{33}$$

and $m_{\mathrm{IV}}^{\mathrm{e}} = 0$.

3. COM of sub-volume IV

For the computation of the COM, we need the filling height $z(t)$ in explicit terms. This can be obtained by solving a third-order equation obtained from equating $m'_{\mathrm{IV}}(t)$ in Eqs. (31) and (33). With $z(t)$ from this procedure, the COM of sub-volume IV (frustum) is given by

$$Z'_{\mathrm{IV}}(t) = \frac{z(t)}{4}\frac{R^2(z) + 2R(z)R_2 + 3R_2^2}{R^2(z) + R(z)R_2 + R_2^2} \tag{34}$$

and $Z_{IV}^{\mathrm{e}} = \lim_{z\to 0} Z'_{\mathrm{IV}} = 0$. Figure 10 shows the functions $Z_{\mathrm{IV}}(t)$ and $m_{\mathrm{IV}}(t)$.

F. Sub-volumes V and VI

The calculations for sub-volumes V and VI (sand stream and lower container) are closely related, therefore we present them together in this section. Sub-volume V is the falling stream bound by the orifice at $z=0$ and the filling level $z_l(t)$ of the lower container. Sub-volume VI consists of the sand resting in the lower container, which is a cylinder of radius R_3 with its bottom at z_3, as shown in Fig. 2. Based on

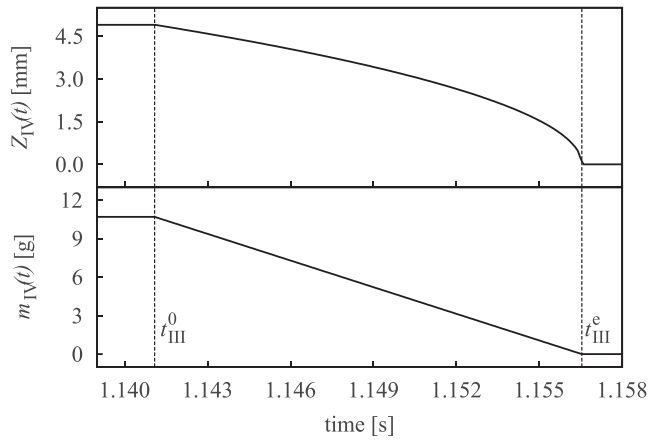

Fig. 10. COM and mass of sub-volume IV as functions of time.

experimental observations, we assume that the upper surface of the sand is flat, due to the large flow rate in our experiment. The same calculation can be performed for any chosen angle of repose at the top of the lower container. The close relation of the sub-volumes V and VI originates in the fact that their common boundary changes with time. Indeed, the surface at vertical position $z_l(t)$ moves upward in time, therefore, despite constant flow rate F the rate of sand settling at the floor is different from F.

1. Density, mass, and COM of the sand stream in general

Particles enter volume V at a certain initial velocity v^*, which follows from continuity between volumes IV and V. Since the flowing sand stream is not confined by lateral walls, here we cannot rely on Beverloo's law[15] of Eq. (5), but rather assume that the flow is proportional to its cross-section and hence that its velocity is given by

$$v^* = -\frac{F}{\rho\pi R_2^2}. \tag{35}$$

At time $t = 0 = t_V^0$, the lid opens and the grains start falling at velocity v^*. Using

$$F = \frac{dm}{dt} = \frac{dm}{dz}\frac{dz}{dt} = \frac{dm}{dz}v(z), \tag{36}$$

we can compute the linear density of the sand stream $\mathrm{d}m/\mathrm{d}z$. The velocity of the grains at vertical position z is

$$v(z) = -\sqrt{(v^*)^2 + 2gz}, \tag{37}$$

and thus

$$\frac{dm}{dz} = -\frac{F}{\sqrt{(v^*)^2 + 2gz}} \qquad 0 \geq z \geq z_l, \tag{38}$$

with the filling height $z_l(t)$ given below.

In terms of the as yet unspecified upper and lower boundaries of the stream, z_L and z_U, respectively, we obtain general equations for the mass of the stream,

$$\begin{aligned} m_{\mathrm{jet}}(z_\mathrm{L}, z_\mathrm{U}) &= \int_{z_\mathrm{L}}^{z_\mathrm{U}} \frac{\mathrm{d}m}{\mathrm{d}z}\mathrm{d}z \\ &= \frac{F}{g}\left[\sqrt{(v^*)^2 + 2gz_\mathrm{U}} - \sqrt{(v^*)^2 + 2gz_\mathrm{L}}\right], \end{aligned} \tag{39}$$

and its COM,

$$\begin{aligned} Z_{\mathrm{jet}}(z_\mathrm{L}, z_\mathrm{U}) = \frac{1}{m_{\mathrm{jet}}(z_\mathrm{L}, z_\mathrm{U})}\int_{z_\mathrm{L}}^{z_\mathrm{U}} z\frac{dm}{dz}dz = -\frac{F}{3g^2\, m_{\mathrm{jet}}(z_\mathrm{L}, z_\mathrm{U})} \\ \times\left[\left(z_\mathrm{L}g - (v^*)^2\right)\sqrt{(v^*)^2 + 2z_\mathrm{L}g}\right. \\ \left. -\left(z_\mathrm{U}g - (v^*)^2\right)\sqrt{(v^*)^2 + 2z_\mathrm{U}g}\right]. \end{aligned} \tag{40}$$

2. Vertical position of the interface $z_l(t)$ between sub-volumes V and VI

Sub-volume VI becomes active when the first grain arrives at the floor at position z_3 at time

$$t_{\mathrm{VI}}^0 = \frac{1}{g}\left(\sqrt{(v^*)^2 + 2gz_3} - v^*\right). \tag{41}$$

For $0 = t_\mathrm{V}^0 \leq t \leq t_{\mathrm{IV}}^\mathrm{e}$, the mass that has flowed through the orifice up to any particular time is either located in the stream or as a sediment in the lower container, so that

$$F\,t = \pi R_3^2 z_l + m_{\mathrm{stream}}(z_l, 0). \tag{42}$$

With Eq. (39) for m_{stream} we obtain a quadratic equation for $z_l(t)$.

3. Mass and COM of sub-volume V (sand stream)

Using the general results from Secs. III F 1 and III F 2, we can compute the evolution of mass and center of mass position of sub-volume V. The scenario is the following: At time $t = 0$, the lid opens and the sand stream gains mass rapidly. The first grain hits the floor at z_3 a short time later. From this moment on, the mass of the stream decreases slowly since the lower filling level z_l increases. When the last grain enters the stream at the orifice, the mass of the stream decreases rapidly and vanishes when the last grain arrives at the top of the sand in the lower container. In quantitative terms:

- For $0 = t_\mathrm{V}^0 \leq t \leq t_{\mathrm{VI}}^0$,

$$\begin{aligned} m'_\mathrm{V}(t) &= m_{\mathrm{stream}}\left(-\frac{g}{2}t^2 + v^*t,\, 0\right) \\ Z'_\mathrm{V}(t) &= Z_{\mathrm{stream}}\left(-\frac{g}{2}t^2 + v^*t,\, 0\right). \end{aligned} \tag{43}$$

- For $t_{\mathrm{VI}}^0 \leq t \leq t_{\mathrm{IV}}^\mathrm{e}$,

$$\begin{aligned} m'_\mathrm{V}(t) &= m_{\mathrm{stream}}(z_l,\, 0) \\ Z'_\mathrm{V}(t) &= Z_{\mathrm{stream}}(z_l,\, 0), \end{aligned} \tag{44}$$

  with $z_l(t)$ given by the solution of Eq. (42).
- For $t_{\mathrm{IV}}^\mathrm{e} \leq t \leq t_\mathrm{V}^\mathrm{e}$,
  at time t_V^e the last grain comes to rest at vertical position $z_l^\mathrm{e} \equiv z_l(t_\mathrm{V}^\mathrm{e})$. The terminal filling height z_l^e is obtained from equating the initial mass of sand in the upper container of the hourglass with the final state, where the sand is contained in the lower container,

$$m_\mathrm{I}^0 + m_{\mathrm{II}}^0 + m_{\mathrm{III}}^0 = m_\mathrm{V}^\mathrm{e} \tag{45}$$

  yielding

$$z_l^\mathrm{e} = z_3 + \frac{R_1^2}{R_3^2}(z_1 - z_2) + \frac{z_2}{3}\frac{R_1^2 + R_1R_2 + R_2^2}{R_3^2}, \tag{46}$$

  and the corresponding time

$$t_\mathrm{V}^\mathrm{e} = t_{\mathrm{VI}}^\mathrm{e} = t_{\mathrm{IV}}^\mathrm{e} + \frac{1}{g}\left(\sqrt{(v^*)^2 + 2g\,z_l^\mathrm{e}} - v^*\right), \tag{47}$$

  with v^* given in Eq. (35).

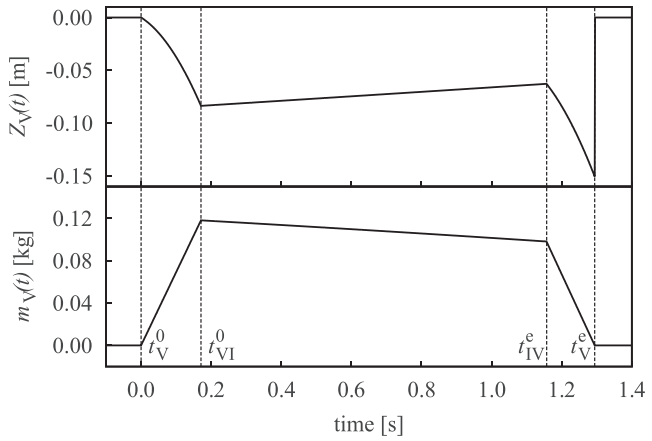

Fig. 11. COM and mass of sub-volume V as functions of time.

For completeness, we add the initial and final values: $m_V^0 = m_V^e = 0$; the COM's Z_V^0 and Z_V^e are both undefined but finite; that is, they do not contribute to the total COM of the system. Figure 11 shows the functions $Z_V(t)$ and $m_V(t)$.

4. Mass and COM of sub-volume VI (lower container)

Sub-volumes V and VI have a common interface at $z_l(t)$, and therefore $t_{VI}^e = t_V^e$. The mass and COM of volume VI can be found directly from the evolution of the lower filling height $z_l(t)$, the solution of Eq. (42). In terms of $z_l(t)$, we then have

$$\begin{aligned} m'_{VI} &= \rho\pi R_3^2[z_l(t) - z_3], \\ Z'_{VI} &= \frac{1}{2}[z_l(t) - z_3]. \end{aligned} \tag{48}$$

The initial and final values are

$$\begin{aligned} m_{VI}^0 &= 0 \\ m_{VI}^e &= m_I^0 + m_{II}^0 + m_{III}^0 \\ Z_{VI}^0 &\equiv \lim_{t\to+t_{VI}^0} Z'_{VI}(t) = z_3 \\ Z_{VI}^e &= \frac{1}{2}\left(z_l^e - z_3\right). \end{aligned} \tag{49}$$

Figure 12 shows the functions $Z_{VI}(t)$ and $m_{VI}(t)$.

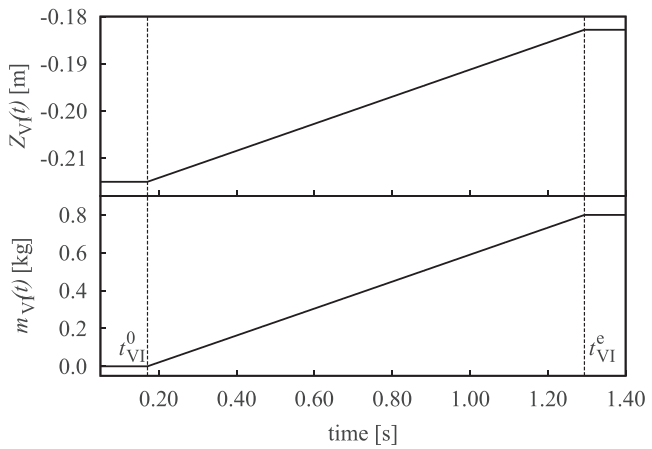

Fig. 12. COM and mass of sub-volume VI as functions of time.

IV. CENTER OF MASS AND WEIGHT OF THE HOURGLASS

The total center of mass $Z(t)$ is obtained via Eq. (1), where the masses and COMs of the sub-volumes are given in the form of Eqs. (3)–(4) with the details for each sub-volume computed in Secs. III B–III F. The solution $Z(t)$ obtained here is rigorous and entirely analytical, albeit given in piecewise form, which makes mathematical operations with this function rather cumbersome. Computer algebra systems such as Maple can be used to conveniently compute the second derivative of this function to obtain the weight F_w of the hourglass via Eq. (2), with the total mass given by $M = m_I^0 + m_{II}^0 + m_{III}^0$.

Figure 13 shows the final result of the analysis: the center of mass $Z(t)$ and the force resulting from its second derivative according to Eq. (2). While $Z(t)$ does not seem impressive, the force shows distinct characteristics that are similar to the experimental data. In particular, we recognize three distinct stages: (i) the initial interval $0 < t \lesssim 0.2$ s, where the stream and the cone develop; (ii) the stage of approximately constant flow, $0.2\,\text{s} \lesssim t \lesssim 1$s; and (iii) the final stage, $t \gtrsim 1$s, when the upper container and the stream run empty and the material comes to rest. In all three stages, we find qualitative and even partially quantitative agreement between theory (solid line) and experiment (dotted line) without employing any adjustable parameters in the model. In particular, in stage (ii) where the textbook solution discussed in the introduction fails, we see good quantitative agreement of theory and experiment.

Despite the overall good agreement of theory and experiment, there are some sizeable local deviations that will be

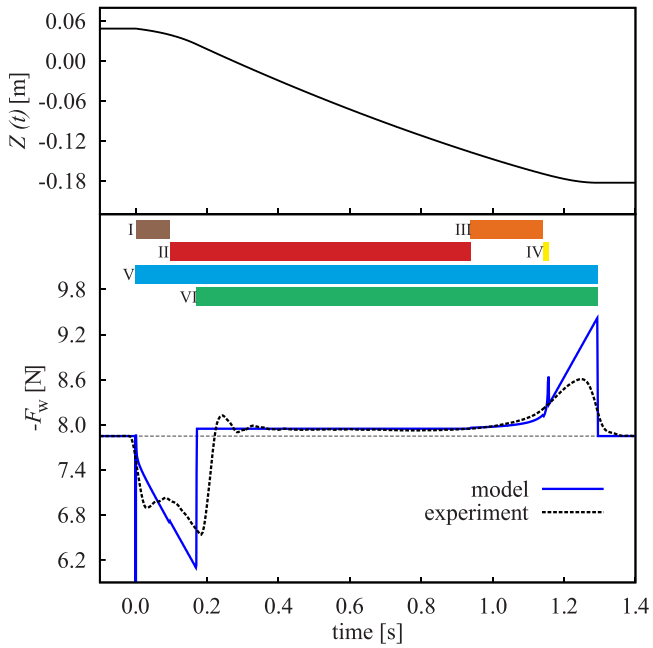

Fig. 13. (color online) COM of the sand flowing in the hourglass as a function of time, and weight of the hourglass due to the flow, according to Eq. (2). The horizontal dashed line shows the weight of the hourglass when the material is at rest. For comparison, the dotted curve shows the experimental result from the experimental setup pictured in Fig. 2. The horizontal bars indicate the intervals of time when the respective sub-volumes are active, (t_i^0, t_i^e) with $i = \{\text{I}, \ldots, \text{VI}\}$. The colors of the bars (online) correspond to the colors in Fig. 2.

discussed in detail. First, we notice a sharp negative peak at $t = 0$ in the theoretical curve, which appears less sharp in the experimental data. The reason for this peak is the assumption that at $t = 0$ the sand starts pouring instantaneously; that is, a finite mass is set into downward motion at finite velocity instantaneously, which implies a δ-function shaped negative acceleration. Looking at the experimental data, we notice that there is a similar behavior, however, the negative peak is of finite value and duration due to the fact that the sand is not set into motion *instantaneously*, but needs a finite time to accelerate. When the total amount of sand is reduced, the mass accelerated at $t = 0$ decreases and the peak gradually disappears. Figure 14 shows the experimentally measured weight in the initial interval $t < 0.22$ s for different amounts of granular material.

Second, at $t \approx 0.25$ s in Fig. 13 we observe a damped oscillation in the experimentally measured weight that does not appear in the theoretical result. The reason for this deviation is the splash of the granular material in a short period after the instant when the stream arrives at the bottom at $t = t^0_{\mathrm{VI}}$. In the theory, we assume that the material comes to rest instantaneously. The movie of the experiment (see video enhancement to Fig. 3 online) shows that this assumption is well justified for the entire experiment, except for a short interval after t^0_{VI}. (A different small oscillation can be seen, e.g., in the interval $0.05\,\mathrm{s} < t < 0.1\,\mathrm{s}$ in Fig. 14, which is due to a resonant frequency of the balance.)

A third significant deviation between experiment and theory can be seen at $t \approx t^{\mathrm{e}}_{\mathrm{VI}}$ when the experiment terminates. While theory predicts an instantaneous drop of the weight, the experiment shows a smooth decay. The reason for this deviation is the assumption of the Beverloo-law constant flow rate F in Eq. (5). According to Janssen's law,[34] the pressure, and thus the flow rate, are independent of the filling height except when the filling height is too small and approaches the size of the orifice or even drops below it. But this is the case for $t \approx t^{\mathrm{e}}_{\mathrm{VI}}$, so that the assumption of constant flow is not justified close to the very end of the experiment. For the same reason (the assumption of constant flow rate), in the interval $(t^0_{\mathrm{VI}}, t^{\mathrm{e}}_{\mathrm{VI}})$ the small positive peak at $t = t^0_{\mathrm{VI}}$ appears in the theory (see the discussion in Sec. III E 1).

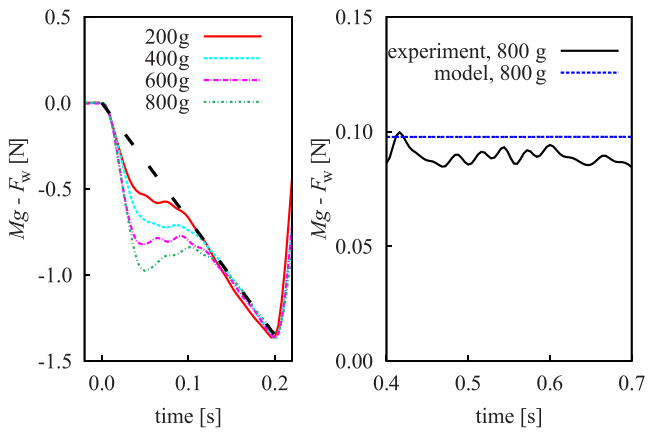

Fig. 14. Left: Experimentally measured weight in the initial time interval $t < 0.22$ s for different amounts of granular material (magnification of Fig. 13). The figure illustrates the appearance of the initial negative peak due to the acceleration of the total amount of granular material after the lid is opened at $t = 0$. Right: Magnification of the plateau in Fig. 13. The deviation of the experimental and theoretical result is about 10%.

The motivation of the division into sub-volumes I to VI is purely to provide a convenient calculation of $M\,d^2Z(t)/dt^2$. This division is by no means unique and so does not lead to any useful physical interpretation of the isolated contributions to F_W. The horizontal bars in Fig. 13 indicate the time intervals, $(t^0_i, t^{\mathrm{e}}_i)$ with $i = \{\mathrm{I}, \ldots, \mathrm{VI}\}$, when the respective sub-volumes are active; that is, when $m_i \neq \mathrm{const}$. Comparison with the curve for the COM and the force $F_W(t)$ shows that an interpretation of the isolated contributions is, at the very least, not straightforward. This is especially true since these contributions cannot exist independently of one another.

From Fig. 2, we see that the sub-volumes are of rather different size. Therefore, one might argue that some of their contributions are negligible and can be disregarded for the computation of F_W. However, recall that the change in weight $F_W - Mg$ follows from the second derivative of $Z(t)$ in Eq. (2). Neglecting any of the sub-volumes would cause non-smoothness of $Z(t)$, at least since summation in Eq. (1) would exclude part of the total. Even for small imperfections of smoothness, the second derivative of $Z(t)$ would reveal wild jumps. We can see such a behavior in Fig. 13 at $t \gtrsim 0$ and $t \approx 1.15$ s due to imperfections of our model assumptions, as discussed above. Although both assumptions do not violate conservation of mass but correspond only to tiny inaccuracies in the flow rate, they leave a clear fingerprint in the force $F_W(t)$. Therefore, we believe that it is necessary to consider the contributions of all sub-volumes before computing the second derivative, even if it requires some technical effort.

V. CONCLUSION

The weight of a running hourglass deviates from the weight of the hourglass at rest due to the accelerated motion of the sand. While this insight is not new (but still not generally acknowledged), in several references it was claimed that the effect is tiny and hardly measurable using standard laboratory equipment. In the present paper, we perform the experiment using very simple equipment and demonstrate quantitative agreement with theory.

While in many cases phenomenological approaches to physics problems are successful, in the case of the weight of an hourglass such an approach is misleading and gives erroneous results that can be found in textbooks and lecture notes. More systematic approaches, such as the one presented here (namely, to consider the acceleration of the center of mass), are certainly more laborious and less elegant. However, they are certainly less prone to fail, which may be considered as the educational message of this paper.

ACKNOWLEDGMENTS

We thank the German Science Foundation (DFG) for funding through the Cluster of Excellence Engineering of Advanced Materials, ZISC and FPS.

[1]At each instant of time, the total weight is a sum of contributions of the material in the upper container, the material in the lower container, the force exerted when the falling sand grains come to rest, thus changing their momentum. Assume at time $t = 0$ the sand starts pouring at constant flow rate $f \equiv dm/dt$. At this time, all sand is in the upper container. The first grain will come to rest at time t_1 in the lower container where it arrives at velocity $v = gt_1$. For $0 \leq t \leq t_1$ the measured mass is $M(t) = M_0 - ft$. For

$t \geq t_1$ we obtain $M(t) = M_0 - ft + f(t - t_1) + \frac{1}{g}\frac{dp}{dt}$, where dp/dt is the rate of momentum change of the pile of sand at the bottom. This momentum change is $d(mv)/dt = m\,dv/dt + v_{\mathrm{rel}}\,dm/dt$, where v_{rel} is the relative speed between the falling grains and the pile at the bottom. Since $dv/dt = 0$ and $v_{\mathrm{rel}} = gt_1$, we end up with $M(t) = M_0 - ft_1 + ft_1 = M_0 = \mathrm{const}$. As a result of this (flawed) solution, we obtain that apart from the very beginning $0 < t < t_1$ and the very end of the flow (where an equivalent calculation can be done), the balance shows M_0, and hence is independent of whether the sand in the hourglass flows or rests. The problem with this calculation is that the accelerated motion of the center of mass is disregarded, and this is what the present paper is about.

[2]K. Y. Shen and Bruce L. Scott, "The hourglass problem," Am. J. Phys. **53**(8), 787–788 (1985).

[3]Ian H. Redmount and Richard H. Price, "The weight of time," Phys. Teach. **36**(7), 432–434 (1998).

[4]Volker Becker and Thorsten Pöschel, "Hourglass of constant weight," Gran. Matter **10**(3), 231–232 (2008).

[5]Fokke Tuinstra and Bouke F. Tuinstra, "The weight of an hourglass," Europhys. News **41**(3), 25–28 (2010).

[6]Bernhard Löffler, "Wann und auf welche Weise beeinflussen suspendierte Teilchen Gewicht und Auftrieb einer Flüssigkeit," Ph.D. thesis, Hohe Philosophische Fakultät der Universität Marburg (1906).

[7]Bernhard Löffler, "Wann und auf welchem Wege beeinflussen suspendierte Teilchen Gewicht und Auftrieb einer Flüssigkeit?," Ann. Phys. **328**(8), 517–531 (1907).

[8]Heinrich Greinacher, *Ergänzungen zur Experimentalphysik. Einführende exakte Behandlung physikalischer Aufgaben, Fragen und Probleme* (Springer, Wien, 1942).

[9]Jearl Walker, *The Flying Circus of Physics* (John Wiley & Sons, Hoboken, 1975).

[10]Walter P. Reid, "Weight of an hourglass," Am. J. Phys. **35**(4), 351–352 (1967).

[11]P. P. Ong, "The wavering weight of the hour-glass," Eur. J. Phys. **11**(3), 188–190 (1990).

[12]J. C. Poggendorff, "Ueber eine Abänderung der Fallmaschine," Ann. Phys. **168**(5), 179–182 (1854).

[13]Luiz Cintra do Prado, "Utilizing automatic balances for Poggendorff's experiment on the second law of motion," Am. J. Phys. **38**(4), 541–542 (1970).

[14]Ricardo Lopes Coelho, P. A. S. Silva, and Paulo de Faria Borges, "On the Poggendorff experiment," Phys. Educ. **50**(6), 667–672 (2015).

[15]W. A. Beverloo, Hendrik Antonie Leniger, and J. van de Velde, "The flow of granular solids through orifices," Chem. Eng. Sci. **15**(3-4), 260–269 (1961).

[16]R. L. Brown, "Minimum energy theorem for flow of dry granules through apertures," Nature **191**(4787), 458–461 (1961).

[17]Metin Yersel, "The flow of sand," Phys. Teach. **38**(5), 290–291 (2000).

[18]Thierry Le Pennec, Knut Jørgen Måløy, Alex Hansen, Madani Ammi, Daniel Bideau, and Xiao-lun Wu, "Ticking hour glasses: Experimental analysis of intermittent flow," Phys. Rev. E **53**(3), 2257–2264 (1996).

[19]Xiao-lun Wu, Knut Jørgen Måløy, Alex Hansen, Madani Ammi, and Daniel Bideau, "Why hour glasses tick," Phys. Rev. Lett. **71**(9), 1363–1366 (1993).

[20]Eirik Manger, Tron Solberg, Bjørn Helge Hjertager, and D. Vareide, "Numerical simulation of the ticking hourglass," Int. J. Multiphase Flow **21**(4), 561–567 (1995).

[21]Christian Veje and Peter Dimon, "Power spectra of flow in an hourglass," Phys. Rev. E **56**(4), 4376–4380 (1997).

[22]Benson K. Muite, Melany L. Hunt, and Gustavo G. Joseph, "The effects of a counter-current interstitial flow on a discharging hourglass," Phys. Fluids **16**(9), 3415–3425 (2004).

[23]Pierre Huber-Burnand, "Ueber das Ausfließen und den Druck des Sandes," Ann. Phys. **92**(6), 316–328 (1829).

[24]Pierre Huber-Burnand, "Über den Ausfluß und den Druck des Sandes," Z. Phys. Math. **6**(1), 95–98 (1829); available at https://books.google.de/books?id=vGoEAAAAYAAJ&pg=PA95&lpg=PA95&dq=Uber+den+Ausfluß+und+den+Druck+des+Sandes&source=bl&ots=_Qv7oDPwBQ&sig=-0AROqGtSjrzGUNeVkMzSr8CsFQ&hl=de&sa=X&ved=0ahUKEwiK5ozFi5zRAhXHd1AKHTONAUwQ6AEIHDAB#v=onepage&q=Uber%20den%20Ausfluß%20und%20den%20Druck%20des%20Sandes&f=false.

[25]Pierre Huber-Burnand, "Lettre de M. Huber-Burnand à M. le professeur Prevost, sur l'écoulment et la pression du sable," Ann. Chim. Phys. **41**, 159–173 (1829); available at http://reader.digitale-sammlungen.de/de/fs1/object/display/bsb10071740_00163.html.

[26]Pierre Huber-Burnand, "Über den Ausfluß und den Druck des Sandes. Schreiben des Hrn. Huber-Burnand an Hrn. Prof. Prevost," Polytech. J. **34**(4), 270–280 (1829); available at http://dingler.culture.hu-berlin.de/article/pj034/ar034071.

[27]Pierre Huber-Burnand, "Lettre de M. Huber-Burnand à M. le professeur Prevost, sur l'écoulment et la pression du sable," Bibliothèque universelle des sciences, belles-lettres, et arts Genève **40**, 22–40 (1829); available at https://hdl.handle.net/2027/pst.000052859786?urlappend=%3Bseq=26.

[28]Pierre Huber-Burnand, "Ueber den Ausfluß und den Druck des Sandes," Kunst- und Gewerbeblatt des Polytechnischen Vereins für das Königreich Bayern **15**(51), 730–740 (1829); available at http://www.mdz-nbn-resolving.de/urn/resolver.pl?urn=urn:nbn:de:bvb:12-bsb10347118-1.

[29]Pierre Huber-Burnand, "Ausfluß des Sandes," in *Repertorium der Experimentalphysik, Enthaltend Eine Vollständige Zusammenstellung der Neuern Fortschritte Dieser Wissenschaft. Als Supplement zu Neuern Lehr- und Wörterbüchern der Physik*, edited by Gustav Theodor Fechner (Leopold Voß, Leipzig, 1832), pp. 82–84.

[30]T. S. Brown (Lieut. of the Corps of Engineers), "Experiments on the resistance of sand to motion through tubes, with especial reference to its use in the blasting of rocks, made at Fort Adams, Newport harbour, under direction of Col. Totten," J. Franklin Inst. State Pennsylvania **18**(7), 1–8 and **18** (8), 73–81 (1836).

[31]Gotthilf Heinrich Ludwig Hagen, "über den Druck und die Bewegung des trockenen Sandes," Bericht über die zur Bekanntmachung geeigneten Verhandlungen der Königlich Preussischen Akademie der Wissenschaften zu Berlin **52**, 35–42 (1852); available at http://bibliothek.bbaw.de/bbaw/bibliothek-digital/digitalequellen/schriften/anzeige/index_html?band=08-verh/1852&seite:int=36.

[32]Philipp Forchheimer, "Über Sanddruck und Bewegungs-Erscheinungen im Inneren trockenen Sandes," Ph.D. thesis (Eberhard-Carls-Universität, Tübingen, 1883).

[33]Brian P. Tighe and Matthias Sperl, "Pressure and motion of dry sand: translation of Hagen's paper from 1852," Gran. Matter **9**(3-4), 141–144 (2007).

[34]H. A. Janssen, "Versuche über Getreidedruck in Silozellen," Z. Ver. Dt. Ing. **39**(35), 1045–1049 (1895).

[35]Ron M. Nedderman, *Statics and Kinematics of Granular Materials* (Cambridge U.P., Cambridge, 1992).

[36]Helmut Fischler and Rezar Corati, "Himmelsblau und Sanduhr: Die heuristische Kraft der Dimensionsanalyse," Phys. Schule **33**(12), 426–429 (1995); available at http://sowiport.gesis.org/search/id/fis-bildung-360312.